Visualizing H2O molecules reacting at TiO2 active sites with transmission electron microscopy

Yuan, Wentao; Zhu, Beien; Li, Xiao Yan; Hansen, Thomas Willum; Ou, Yang; Fang, Ke; Yang, Hangsheng; Zhang, Ze; Wagner, Jakob Birkedal; Gao, Yi

Total number of authors:
11

Published in:
Science

Link to article, DOI:
10.1126/science.aay2474

Publication date:
2020

Document Version
Peer reviewed version

Visualizing H_2O molecules reacting at TiO_2 active sites with transmission electron microscopy

Wentao Yuan[1†], Beien Zhu[2, 4†], Xiao-Yan Li[2, 5†], Thomas W. Hansen[3], Yang Ou[1], Ke Fang[1], Hangsheng Yang[1], Ze Zhang[1*], Jakob B. Wagner[3*], Yi Gao[2, 4*] and Yong Wang[1*]

[1] State Key Laboratory of Silicon Materials and Center of Electron Microscopy, School of Materials Science and Engineering, Zhejiang University, Hangzhou, 310027 China

[2] Division of Interfacial Water and Key Laboratory of Interfacial Physics and Technology, Shanghai Institute of Applied Physics, Chinese Academy of Sciences, Shanghai, 201800 China

[3] DTU Nanolab, Technical University of Denmark, DK-2800, Kgs. Lyngby, Denmark

[4] Shanghai Advanced Research Institute, Chinese Academy of Sciences, Shanghai, 201210 China

[5] University of Chinese Academy of Sciences, Beijing, 100049 China

*Correspondence to: yongwang@zju.edu.cn (Yong Wang); gaoyi@zjlab.org.cn (Yi Gao); jakob.wagner@cen.dtu.dk (Jakob Wagner); zezhang@zju.edu.cn (Ze Zhang)

† These authors contributed equally.

Abstract: Imaging a reaction taking place at the molecular level could provide the most direct information for understanding catalytic reaction mechanism. We used nanocrystalline anatase TiO_2 (1×4)-(001) surface as a catalyst, which provided highly ordered Ti_{4c} "active rows" to realize real-time monitoring of H_2O molecules dissociating and reacting on the catalyst surface with in-situ environmental transmission electron microscopy. The twin-protrusion configuration of adsorbed H_2O was observed. During the water-gas-shift reaction, dynamic changes in these structures were visualized on these active rows at the molecular level.

One Sentence Summary: Visualization of H_2O molecules reacting at active sites of TiO_2 surface at the molecular level was realized via ETEM.

Imaging at the atomic scale with transmission electron microscopy (TEM) has benefited from the developments of aberration corrector and in situ equipment (*1-8*). For studies of heterogeneous catalysts, these developments, along with approaches that allow gases and even liquids to contact samples (environmental TEM or ETEM) have enabled imaging of single molecules and atoms adsorbed on catalyst surface (*9-14*). However, the direct visualization of gas molecules reacting at catalytic sites is generally challenging for TEM. Normally, the molecules that adsorb and react dynamically do not offer sufficient contrast for TEM identification. We now show that this obstacle could be overcome by taking advantage of the highly ordered four-coordinated Ti (Ti_{4c}) rows ("active rows", because of the lower coordination) on the anatase TiO_2 (1×4)-(001) surface, which ensured enhanced contrast of adsorbing molecules along the row direction to allow real-time monitoring of H_2O species dissociating and reacting on the catalyst surface.

The atomic structure of TiO_2 (1×4)-(001) surface has been characterized by both aberration-corrected ETEM and scanning transmission electron microscopy (STEM) images. The bulk-truncated (1×1)-(001) surface usually reconstructs to a (1×4)-(001) surface (Fig. 1, A to C) by periodically replacing the surface oxygen rows (along [010] direction) with TiO_3 ridges every four-unit cell along TiO_2 [100] direction (*15-17*). As a result, protruded Ti_{4c} rows are periodically exposed on the surface and show distinct contrast, so the subtle changes occurring in reactions could be detected in ETEM observation without contrast overlap. The ordered Ti_{4c} "active rows" could provide sufficient contrast for direct ETEM visualization of water if it adsorbed in ordered arrays.

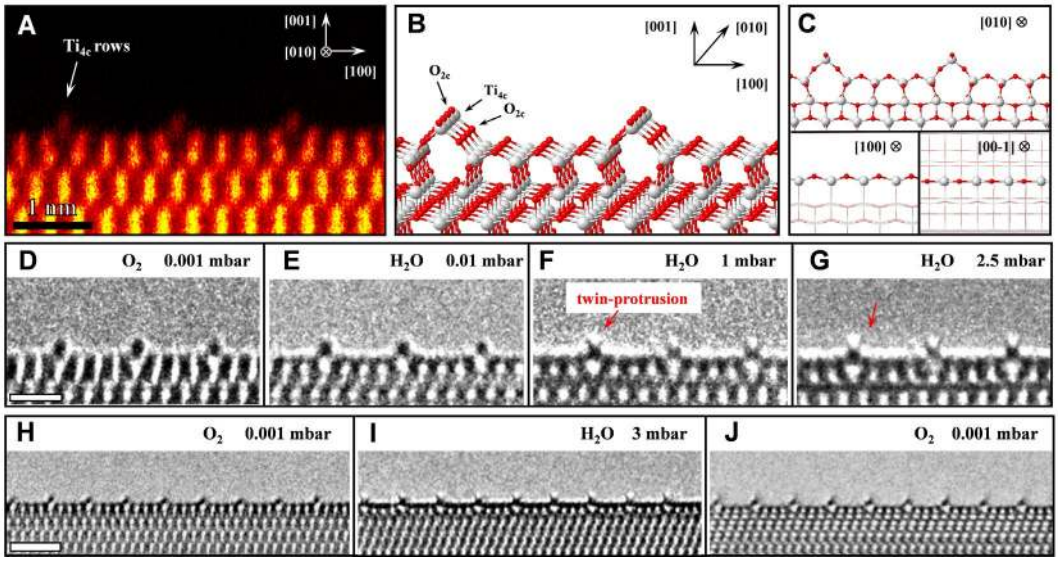

Figure 1. The dynamic atomic structural evolution of (1×4) reconstructed TiO_2 (001) surface under water vapor environment. (**A**) HAADF-STEM image of (1×4)-(001) surface, viewed from [010] direction. The image was acquired at 700 °C in vacuum (TEM column pressure: ~10^{-7} mbar). (**B**) Ad-molecule (ADM) reconstruction models of the (1×4)-(001) surface. (Ti, gray; O, red) (**C**) atomic model of Ti_{4c} row. (**D-G**) Aberration-corrected in situ ETEM images show the same area of TiO_2 (001) surface at 700 °C under oxygen (D, 0.001 mbar) and water vapor conditions (E, 0.01 mbar; F, 1 mbar; G, 2.5 mbar). The scale bar indicates 1 nm. (**H-J**) another case shows the reversible structural change induced by the changing of gas environment at 700 °C, from oxygen (H, 0.001 mbar) to water vapor (I, 3 mbar), and revert to oxygen (J, 0.001 mbar). The scale bar indicates 2 nm.

We synthesized TiO_2 nanocrystals with exposed {001} facets by a hydrothermal route (see supplementary materials) (*18, 19*). The nanocrystals were heated in oxygen in situ (~10^{-3} mbar) at 500 to 700 °C to trigger the reconstruction. The reconstructed structures remained stable in this temperature range, in accord with recent studies in ETEM (*15, 16, 20*). During the ETEM experiments, we used a constant electron beam dose with a small value (< 1 A/cm^2), and no

appreciable irradiation damage was observed on TiO_2 surface (*21*). After heating at 700 °C for ~10 mins, the reconstructed TiO_2 (1×4)-(001) surface of an ad-molecule (ADM) configuration was obtained, as confirmed by the ETEM image (Fig. 1D) where the protruding black dots represent the Ti_{4c} rows. The ADM structure did not show appreciable change after ~16 mins of intermittent TEM observation.

The O_2 gas was then evacuated and H_2O vapor (Fig. S1) was introduced at the same temperature. When the H_2O pressure was raised to 1 mbar, two additional small protrusions were observed at the top of the Ti_{4c} rows (Fig. 1F). This twin-protrusion structure became more resolved for a H_2O pressure to 2.5 mbar due to a higher water coverage (Fig. 1G and Movie S1). At both pressures, the twin-protrusion structure kept visible during the TEM observation. When the background environment was changed from H_2O to O_2 or vacuum, the twin-protrusion structure disappeared (Fig. 1, H and J; Fig. S2). If we kept the electron beam off after acquiring Fig. 1H and then introduced H_2O, a snapshot (Fig. 1I) obtained ~ 5 mins later still showed twin-protrusion structure, which excludes the effect of electron beam in its formation. We also excluded the defocus effect of TEM imaging in different gas environments (Figs. S3-S5). Because there was no other structural change of the TiO_2 surface, we attributed the twin protrusions to an adsorbed water species.

We performed in situ Fourier transform infrared spectroscopy (FTIR) to characterize the surface adsorption species. We heated the TiO_2 crystals to 500 °C in vacuum to obtain the (1×4)-(001) surface. Under these conditions, no obvious valley was observed in the hydroxyl region (blue line in Fig. 2A). Water vapor (5 mbar) was introduced into the in situ FTIR reactor to mimic the in situ TEM experimental condition. ~20 minutes later, we started to acquire spectrum and observed two valleys at hydroxyl region at 3717 and 3663 cm^{-1}. We assigned both features to the adsorbed species on the Ti_{4c} rows (*22, 23*) because previous studies show that the water molecules only

chemically adsorb at the Ti_{4c} ridges on the (1×4)-(001) surface (*24*). It indicates that the twin-protrusion structure observed in the ETEM experiments (also at 500 ºC, refer to Fig. S6) was composed of two different hydroxyl species.

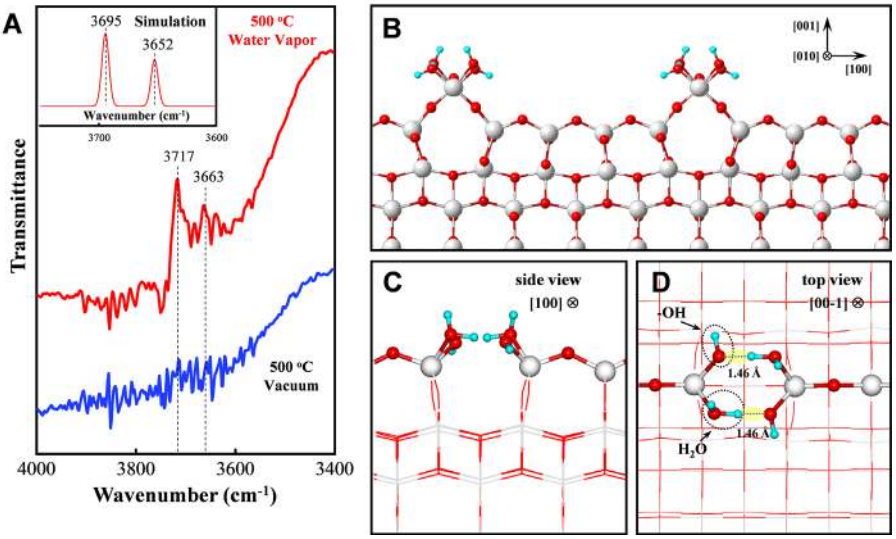

Figure 2. (**A**) In situ FTIR spectra of hydroxyl region are shown for TiO_2 in the presence of water vapor (5 mbar; 500 °C) and vacuum (10^{-6} mbar; 500 °C). (**B** to **D**) Atomic structure of the adsorbed H_2O species on the TiO_3 rows verified by theoretical calculations, viewed from [010] direction (B). [100] direction (C), and [00-1] direction (D) (gray, Ti; red, O; cyan, H).

We used density functional theory (DFT) to examine the different adsorbed water structures on the (1×4)-(001) surface (Fig. S7, Fig. S8 and Appendix S1). At low coverage, one dissociative H_2O adsorbs stably at the Ti_{4c} site by transforming the H atom to the adjacent O_{2c} atom and cleaving the Ti_{4c}-O_{2c} bond. With increasing coverage, the stability of dissociatively adsorbed H_2O structure decreases because of the increased stress in the reconstructed substrate, which agrees recently reported results (*25*). Instead, the relative stability of the structure with two symmetric

protrusions (each is an OH-H_2O group (Figs. 2, B to D) increases because it does not induce additional stress at higher coverages (Fig. S9). It has comparable adsorption energy per H_2O with the dissociatively adsorbed H_2O at 1/2 coverage. The stability of this twin-protrusion structure becomes compelling when the coverage reaches 1, which corresponds to the experimental condition as calculated by combining the adsorption energy with the thermodynamic adsorption isotherm (*26, 27*). Based on this atomic structure, a simulated HRTEM image (Fig. S10B) was generated that agreed with the ETEM image (Fig. S10A), and the calculated vibration frequencies of the twin-protrusion at 3695 and 3652 cm^{-1}, respectively, were in good consistence with the in situ FTIR results.

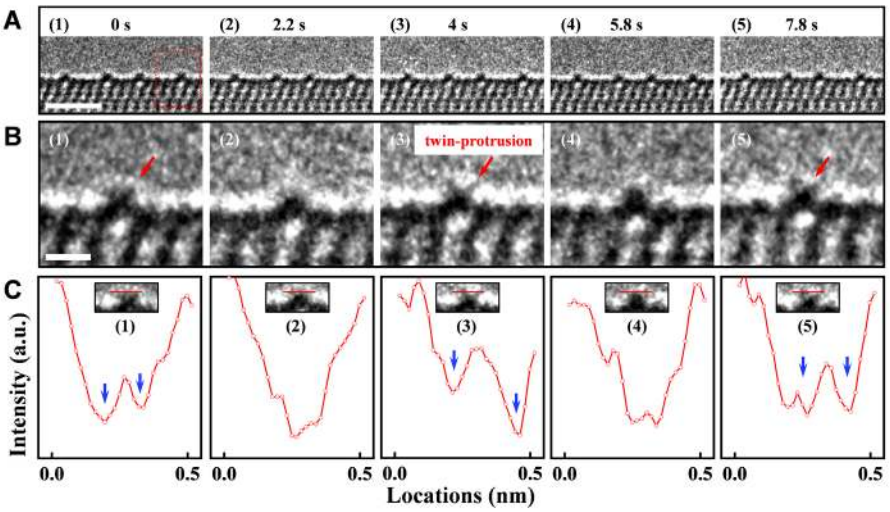

Figure 3. (**A**) Sequential ETEM images show the dynamic structural evolution of (1×4)-(001) surface under the mixed gas environment (CO and H_2O vapor; 1:1; gas pressure: 5 mbar; temperature 700 °C), viewed from [010] direction. The scale bar indicates 2 nm. (**B**) The enlarged ETEM images show the dynamic structural evolution of the Ti row marked by the dotted rectangle of (A). The scale bar indicates 0.5 nm. (**C**) Intensity profiles along the lines crossed the Ti rows of (B). The blue arrows point to the intensity valleys corresponding to the "twin-protrusions."

Because TiO_2 can catalyze the water-gas-shift (WGS) reaction ($H_2O + CO \rightarrow H_2 + CO_2$) at elevated temperatures (*28, 29*), we studied this reaction by introducing CO into the ETEM column. The gas environment was changed from the pure water vapor (2.5 mbar) to a mixed gas environment (CO and H_2O vapor; 1:1; pressure: 5 mbar). Under these conditions, the twin-protrusion structure became unstable (Fig. 3A, Movie S2). Its contrast changed dynamically. Most of the time it was blurred but would occasionally clear (Fig. 3B), with no substantial contrast change observed in TiO_2 bulk and in other surface areas. For example in one case, initially the twin-protrusion was clearly seen [Fig. 3B(1)], almost disappeared after 2.2 s [Fig. 3B(2)], and then reappeared at 4 s [Fig. 3B(3)]. The disappearance and reappearances occurred again at 5.8 s [Fig. 3B(4)] and 7.8 s [Fig. 3B(5)], respectively. The contrast change of the twin-protrusions was also evidenced by the intensity profiles across the protruding row (Fig. 3C). Similar cases are shown in Fig. S11 and Movie S3. In a pure water vapor environment, the twin-protrusions did not show such contrast changes (Fig. S12 and Movie S1), which excludes electron beam effects for the disappearance and reappearances.

Thus, the dynamic change of twin-protrusions under mixture gas environments suggests the adsorbed hydroxyls were reacting with CO molecules, which directly shows that the Ti_{4c} sites are the reaction sites. In addition, because the net free energy change of this reaction is negative (-3.76 kJ mol^{-1} under the experimental condition) and the known conversion temperatures are generally lower than 700 °C (*28, 29*), it is reasonable to conclude that the observed reaction was not induced by the election-beam. The reaction pathway of the twin-protrusion adsorbed H_2O species with CO molecules was calculated by DFT (Fig. S13). During the reaction, the H_2O species of the twin-protrusion are consumed by CO gas and supplemented by H_2O vapor repeatedly, which relates to

the dynamic contrast change observed in experiments. In the reaction cycle (Fig. S13), the two largest energy barriers come from H_2O dissociation of the twin-protrusion (0.48 eV) and single-OH-H_2O (0.57 eV) structures, which makes them two relatively stable structures in the reaction with relatively long lifetimes. Thus, a changing mixture of single-OH-H_2O and twin-protrusion structures were imaged in TEM. The contrast of the twin-protrusions would occasionally clear when they were the majority on one of the active rows [Figs. 3B(2) and 3B(4)]. Most of the time, the contrast is blurred because of the interference between the two structures [Figs. 3B(1), 3B(3) and 3B(5)]. The single-OH-H_2O structure was not obvious in TEM, as shown by the simulated image (Fig. S14).

By visualizing and monitoring the adsorbed water species on the ridge of the (1×4)-(001) TiO_2 surface, we confirmed directly the Ti_{4c} atoms on the ridge are active sites for H_2O dissociation and reaction. The direct TEM visualization revealed an adsorbed water structure on the TiO_2 surface with a twin-protrusion feature. This work demonstrates that the in situ ETEM can be used to monitor a catalytic process taking place at highly ordered active sites.

REFERENCES AND NOTES

1. D. A. Muller, Structure And Bonding at The Atomic Scale by Scanning Transmission Electron Microscopy. *Nature Materials* **8**, 263 (2009).
2. D. S. Su, B. S. Zhang, R. Schlogl, Electron Microscopy of Solid Catalysts-Transforming from a Challenge to a Toolbox. *Chemical Reviews* **115**, 2818-2882 (2015).
3. L. DeRita, J. Resasco, S. Dai, A. Boubnov, H. V. Thang, A. S. Hoffman, I. Ro, G. W. Graham, S. R. Bare, G. Pacchioni, X. Pan, P. Christopher, Structural Evolution of Atomically Dispersed Pt Catalysts Dictates Reactivity. *Nature Materials* ***18****, 746-751 (2019).*

4. L. Luo, M. Su, P. Yan, L. Zou, D. K. Schreiber, D. R. Baer, Z. Zhu, G. Zhou, Y. Wang, S. M. Bruemmer, Z. Xu, C. Wang, Atomic Origins of Water-Vapour-Promoted Alloy Oxidation. *Nature Materials* **17**, 514-518 (2018).

5. L. F. Zou, C. M. Yang, Y. K. Lei, D. Zakharov, J. M. K. Wiezorek, D. Su, Q. X. Yin, J. Li, Z. Y. Liu, E. A. Stach, J. C. Yang, L. Qi, G. F. Wang, G. W. Zhou, Dislocation Nucleation Facilitated by Atomic Segregation. *Nature Materials* **17**, 56 (2017).

6. L. X. Zhang, B. K. Miller, P. A. Crozier, Atomic Level In Situ Observation of Surface Amorphization in Anatase Nanocrystals During Light Irradiation in Water Vapor. *Nano Letters* **13**, 679-684 (2013).

7. K. Sytwu, F. Hayee, T. C. Narayan, A. L. Koh, R. Sinclair, J. A. Dionne, Visualizing Facet-Dependent Hydrogenation Dynamics in Individual Palladium Nanoparticles. *Nano Letters* **18**, 5357-5363 (2018).

8. Y. Y. Lin, J. G. Wen, L. H. Hu, R. M. Kennedy, P. C. Stair, K. R. Poeppelmeier, L. D. Marks, Synthesis-Dependent Atomic Surface Structures of Oxide Nanoparticles. *Physical Review Letters* **111**, 156101 (2013).

9. C. L. Jia, M. Lentzen, K. Urban, Atomic-Resolution Imaging of Oxygen in Perovskite Ceramics. *Science* **299**, 870-873 (2003).

10. M. Koshino, T. Tanaka, N. Solin, K. Suenaga, H. Isobe, E. Nakamura, Imaging of Single Organic Molecules in Motion. *Science* **316**, 853 (2007).

11. Z. Liu, K. Yanagi, K. Suenaga, H. Kataura, S. Iijima, Imaging the Dynamic Behaviour of Individual Retinal Chromophores Confined inside Carbon Nanotubes. *Nature Nanotechnology* **2**, 422 (2007).

12. J. E. Allen, E. R. Hemesath, D. E. Perea, J. L. Lensch-Falk, Z. Y. Li, F. Yin, M. H. Gass, P. Wang, A. L. Bleloch, R. E. Palmer, L. J. Lauhon, High-Resolution Detection of Au Catalyst Atoms in Si Nanowires. *Nature Nanotechnology* **3**, 168 (2008).

13. Y. Oshima, Y. Hashimoto, Y. Tanishiro, K. Takayanagi, H. Sawada, T. Kaneyama, Y. Kondo, N. Hashikawa, K. Asayama, Detection of Arsenic Dopant Atoms in a Silicon Crystal Using a Spherical Aberration Corrected Scanning Transmission Electron Microscope. *Physical Review B* **81**, 035317 (2010).

14. H. Yoshida, Y. Kuwauchi, J. R. Jinschek, K. J. Sun, S. Tanaka, M. Kohyama, S. Shimada, M. Haruta, S. Takeda, Visualizing Gas Molecules Interacting with Supported Nanoparticulate Catalysts at Reaction Conditions. *Science* **335**, 317-319 (2012).

15. W. T. Yuan, H. L. Wu, H. B. Li, Z. X. Dai, Z. Zhang, C. H. Sun, Y. Wang, In Situ STEM Determination of the Atomic Structure and Reconstruction Mechanism of the TiO_2 (001) (1 × 4) Surface. *Chemistry of Materials* **29**, 3189-3194 (2017).

16. W. T. Yuan, Y. Wang, H. B. Li, H. L. Wu, Z. Zhang, A. Selloni, C. H. Sun, Real-Time Observation of Reconstruction Dynamics on TiO_2 (001) Surface under Oxygen via an Environmental Transmission Electron Microscope. *Nano Letters* **16**, 132-137 (2016).

17. M. Lazzeri, A. Selloni, Stress-Driven Reconstruction of an Oxide Surface: The Anatase TiO_2 (001)-(1×4) Surface. *Physical Review Letters* **87**, 266105 (2001).
18. H. G. Yang, C. H. Sun, S. Z. Qiao, J. Zou, G. Liu, S. C. Smith, H. M. Cheng, G. Q. Lu, Anatase TiO_2 Single Crystals With a Large Percentage of Reactive Facets. *Nature* **453**, 638-641 (2008).
19. X. G. Han, Q. Kuang, M. S. Jin, Z. X. Xie, L. S. Zheng, Synthesis of Titania Nanosheets with a High Percentage of Exposed (001) Facets and Related Photocatalytic Properties. *Journal of the American Chemical Society* **131**, 3152-3153 (2009).
20. K. Fang, G. X. Li, Y. Ou, W. T. Yuan, H. S. Yang, Z. Zhang, Y. Wang, An Environmental Transmission Electron Microscopy Study of the Stability of the TiO_2 (1×4) Reconstructed (001) Surface. *The Journal of Physical Chemistry C* **123**, 21522-21527 (2019).
21. Y. Kuwauchi, H. Yoshida, T. Akita, M. Haruta, S. Takeda, Intrinsic Catalytic Structure of Gold Nanoparticles Supported on TiO_2. *Angewandte Chemie-International Edition* **51**, 7729-7733 (2012).
22. C. Arrouvel, M. Digne, M. Breysse, H. Toulhoat, P. Raybaud, Effects of Morphology on Surface Hydroxyl Concentration: A DFT Comparison of Anatase-TiO_2 and Gamma-Alumina Catalytic Supports. *Journal of Catalysis* **222**, 152-166 (2004).
23. C. Deiana, E. Fois, S. Coluccia, G. Martra, Surface Structure of TiO_2 P25 Nanoparticles: Infrared Study of Hydroxy Groups on Coordinative Defect Sites. *The Journal of Physical Chemistry C* **114**, 21531-21538 (2010).
24. J. Blomquist, L. E. Walle, P. Uvdal, A. Borg, A. Sandell, Water Dissociation on Single Crystalline Anatase TiO_2 (001) Studied by Photoelectron Spectroscopy. *Journal Of Physical Chemistry C* **112**, 16616-16621 (2008).
25. I. Beinik, A. Bruix, Z. Li, K. C. Adamsen, S. Koust, B. Hammer, S. Wendt, J. V. Lauritsen, Water Dissociation and Hydroxyl Ordering on Anatase TiO_2 (001)-(1×4). *Physical Review Letters* **121**, 206003 (2018).
26. M. Y. Duan, J. Yu, J. Meng, B. Zhu, Y. Wang, Y. Gao, Reconstruction of Supported Metal Nanoparticles in Reaction Conditions. *Angewandte Chemie International Edition* **57**, 6464-6469 (2018).
27. B. Zhu, Z. Xu, C. Wang, Y. Gao, Shape Evolution of Metal Nanoparticles in Water Vapor Environment. *Nano Letters* **16**, 2628-2632 (2016).
28. P. Panagiotopoulou, D. I. Kondarides, Effect of Morphological Characteristics of TiO_2-Supported Noble Metal Catalysts on Their Activity for the Water–Gas Shift Reaction. *Journal of Catalysis* **225**, 327-336 (2004).
29. D. G. Rethwisch, J. A. Dumesic, The Effects of Metal-Oxygen Bond Strength on Properties of Oxides: II. Water-Gas Shift over Bulk Oxides. *Applied Catalysis* **21**, 97-109 (1986).
30. J. M. Li, D. S. Xu, Tetragonal faceted-nanorods of anatase TiO2 single crystals with a large percentage of active {100} facets. *Chemical Communications* **46**, 2301-2303 (2010).

31. N. de Jonge, F. M. Ross, Electron microscopy of specimens in liquid. *Nature Nanotechnology* **6**, 695-704 (2011).
32. T. W. Hansen, J. B. Wagner, Eds., Controlled Atmosphere Transmission Electron Microscopy. (Springer, Switzerland, 2016).
33. G. Kresse, J. Hafner, Ab Initio Molecular Dynamics for Liquid Metals. *Physical Review B* **47**, 558-561 (1993).
34. G. Kresse, J. Furthmüller, Efficient Iterative Schemes for Ab Initio Total-Energy Calculations using a Plane-Wave Basis Set. *Physical Review B* **54**, 11169-11186 (1996).
35. P. E. Blöchl, O. Jepsen, O. K. Andersen, Improved Tetrahedron Method for Brillouin-Zone Integrations. *Physical Review B* **49**, 16223-16233 (1994).
36. G. Kresse, D. Joubert, From Ultrasoft Pseudopotentials to the Projector Augmented-Wave Method. *Physical Review B* **59**, 1758-1775 (1999).
37. J. P. Perdew, K. Burke, M. Ernzerhof, Generalized Gradient Approximation Made Simple. *Physical Review Letters* **77**, 3865-3868 (1996).
38. H. J. Monkhorst, J. D. Pack, Special Points for Brillouin-Zone Integrations. *Physical Review B* **13**, 5188-5192 (1976).
39. G. Henkelman, B. P. Uberuaga, H. Jónsson, A Climbing Image Nudged Elastic Band Method for Finding Saddle Points and Minimum Energy Paths. *The Journal of Chemical Physics* **113**, 9901-9904 (2000).
40. P. Giannozzi and S. Baroni, Vibrational and Dielectric Properties of C60 from Density-Functional Perturbation Theory. *The Journal of Chemical Physics* **100**, 8537-8539 (1994).
41. P. L. Hansen, J. B. Wagner, S. Helveg, J. R. Rostrup-Nielsen, B. S. Clausen, H. Topsøe, Atom-Resolved Imaging of Dynamic Shape Changes in Supported Copper Nanocrystals. *Science* **295**, 2053 (2002).
42. S. Helveg, C. F. Kisielowski, J. R. Jinschek, P. Specht, G. Yuan, H. Frei, Observing Gas-Catalyst Dynamics at Atomic Resolution and Single-Atom Sensitivity. *Micron* **68**, 176-185 (2015).

ACKNOWLEDGMENTS:

We gratefully acknowledge the support and useful discussions from Prof. Jie Fan (Department of Chemistry, Zhejiang University). **Funding:** We acknowledge the financial support of National Natural Science Foundation of China (51390474, 91645103, 11574340, 21773287, 51801182, 11604357 51872260, and 11327901), the Zhejiang Provincial Natural Science Foundation (LD19B030001), the Ministry of Science and Technology of China (2016YFE0105700) and the Fundamental Research Funds for the Central Universities. B.Z. thanks for Natural Science Foundation of Shanghai (16ZR1443200) and the Youth Innovation Promotion Association CAS. The computations were performed on Guangzhou and Shanghai supercomputer centers. W.Y. thanks for China Postdoctoral Science Foundation (2018M642407, 2019T120502).

Author Contributions: Y.W. initiated the work. Y.W., Y. G., J. W. and Z. Z. supervised the work. W. Y., Y. O. and K. F. synthesized the samples. W.Y. and T. H. conducted the ETEM experiments. Y. O. and H. Y. carried out the in-situ FTIR experiments. B. Z. and X. L. performed the calculations. All authors participated in the analysis and discussion. W.Y., B. Z. and X. L. contributed equally to this work.

Competing interests: The authors declare no competing financial interests.

Data and materials availability: All (other) data needed to evaluate the conclusions in the paper are present in the paper, the Supplementary Materials, the Appendix or the Cambridge Crystallographic Data Centre (Deposition Number: CSD 1970465-1970473).

SUPPLEMENTARY MATERIALS:

Materials and Methods

Supplementary Text

Figures S1-S14

References (30-42)

Movies S1-S3

Appendix S1

Databases S1-S9